Front. Chem. China 2011, 6(4): 287–299
DOI 10.1007/s11458-011-0259-0

RESEARCH ARTICLE

Theoretical study on the hydration of hydrogen peroxide in terms of *ab initio* method and atom-bond electronegativity equalization method fused into molecular mechanics

Chunyang YU (✉), Lidong GONG (✉) and Zhongzhi YANG (✉)

In this paper, the interaction between hydrogen peroxide (HP) and water were systemically studied by atom-bond electronegativity equalization method fused into molecular mechanics (ABEEM/MM) and *ab initio* method. The results show that the optimized geometries, interaction energies and dipole moments of hydrated HP clusters $HP(H_2O)_n$ (n = 1–6) calculated by ABEEM/MM model are fairly consistent with the MP2/aug-cc-pVTZ//MP2/aug-cc-pVDZ results. The ABEEM/MM results indicate that n = 4 is the transition state structure from 2D planar structure to 3D network structure. The variations of the average hydrogen bond length with the increasing number of water molecules given by ABEEM/MM model agree well with those of *ab initio* studies. Moreover, the radial distribution functions (RDFs) of water molecule around HP in HP aqueous solution have been analyzed in detail. It can be confirmed that HP is a good proton donor and poor proton acceptor in aqueous solution by analysis of the RDFs.

Keywords ABEEM/MM model, *ab initio* calculation, hydrogen peroxide, water

1 Introduction

Hydrogen peroxide (HP) is a substance that plays an important role in atmospheric chemistry, biology, biochemistry, environmental chemistry and medicine [1–11]. It is a dominant oxidant in clouds, fog, and rain, affecting the aqueous oxidation of SO_2 [10]. It is a byproduct of several metabolic pathways, giving significant quantities of HP detectable in the human blood [11]. It is also used medicinally, in the form of a 3% aqueous solution, as an antiseptic and throat wash. On the other hand, it is interesting as one of the simplest molecules for which internal rotation can take place.

In recent years, a number of theoretical work has been devoted to the study of small $H_2O_2(H_2O)_n$ complexes [12–19]. The rotational barrier of hydrogen peroxide in hydrogen bonded structure of H_2O_2–H_2O complexes in gas and solution phase have been studied by Du et al. [13]. *Ab initio* studies due to Dobado and Molina [17] reported three minima and two transition state structures for H_2O_2–H_2O complexes. They estimated the binding energy of this heterocluster to be (6.4±0.2) kcal/mol, typical of hydrogen bonded complexes. Mo et al. [19] carried out investigations on structures, vibrational frequencies and thermodynamic properties of the H_2O_2–H_2O complex. According to those work the global minimum of H_2O_2–H_2O at both the restricted Hartree-Fock (RHF) and MP2 levels is a five-membered ring, comprising both covalent and hydrogen bonds. The structures as well as thermodynamic properties of $H_2O_2(H_2O)_n$ (n = 1–3) have been studied by Ju et al. [16]. Those results indicated that the polarity of the solvent has played an important role on the structures, relative stabilities and rotational barriers of different isomers. Kulkarni et al. have performed extensive quantum chemical studies on $H_2O_2(H_2O)_n$ (n = 1–6) [14] and $(H_2O_2)_2(H_2O)_n$ (n = 1–2) [15] at HF and MP2 levels of theory. The structures of these complexes once again show a close structural resemblance with the corresponding $(H_2O_2)_n$ as well as $(H_2O)_n$ clusters. Comparison of the electronic excitation and ionization of $H_2O_2(H_2O)_n$ (n = 1–6) with $(H_2O)_n$ (n = 1–7) clusters has been investigated by Ferreira et al. [20]. Their studies provided useful data to assess how a reactive oxidative species presents in water clusters from an electronic point of view. Furthermore, computational studies in the condensed phase have been reported, including a quantum chemical investigation on the interaction with ice surface model [21], as well as classical simulations of HP dissociation in supercritical water [22] or adsorption at the air/water interface [23]. Recently, Martins-Costa and Ruiz-López [24] have investigated hydrogen peroxide in aqueous solution using combined quantum/classical force field.

On the basis of the electronegativity equalization method (ABEEM), the fluctuating charge models in combination with molecular mechanics have been widely developed in the past few years [25–44]. Rick and Berne [28] have developed dynamical fluctuating charge (FQ) force field to study the

Received October 27, 2011; accepted November 9, 2011
School of Chemistry and Chemical Engineering, Liaoning Normal University, Dalian 116029, China
E-mail: chunyangyu@163.com, gongjw@lnnu.edu.cn, zzyang@lnnu.edu.cn

liquid water; Patel et al. [37] have developed CHARMM FQ force field, which is applied to the protein simulations. Based on the atom-bond electronegativity equalization method [45–47] fused into molecular mechanics (MM), Yang et al. [48–59] have developed a new polarizable force field, i.e., ABEEM/MM fluctuating charge model. It has been applied successfully to the water system [48,49], ion-water system [50–52], organic molecules [53], peptides [54], nucleic acid system [55–57] and proteins [58]. Recently, we have constructed a new ABEEM/MM potential for HP system [59], and successfully applied it to gas-phase HP clusters and liquid-state HP.

The primary of this paper is to carry out a systemic study on the hydration of HP in terms of a high-level *ab initio* methods and ABEEM/MM polarizable force field. The essence of this model is to employ the ABEEM charges of all atoms, bonds, and lone-pairs electrons of the system into the calculation of electrostatic interaction term. First, conformations associated with the $H_2O_2(H_2O)_n$ (n = 1–6) are searched by the *ab initio* method. Then, we will construct an ABEEM/MM interaction potential for the HP-water system, and reliability of this potential will be confirmed in view of the comparison of the hydrated HP clusters with QM calculations. Furthermore, the structural properties of HP aqueous solution will be investigated by classical molecular dynamics simulation. The remainder of this article is arranged as follows. In section 2, the theoretical methods are briefly introduced. In section 3, we will present the results and discussions of the static properties for $H_2O_2(H_2O)_n$ (n = 1–6) clusters and the structural properties of HP aqueous solution. Finally, a brief conclusion will be given.

2 Methodology

2.1 Quantum mechanical calculations

The quantum mechanical calculations were performed on an SGI Altix 3700 server by using the Gaussian 03 [60] program package. Geometries were optimized at the MP2/aug-cc-pVDZ level with and without counterpoise correction [61] (using OPT = tight and SCF = tight keywords), respectively. Energies were determined on the MP2/aug-cc-pVTZ level with basis set superposition error (BSSE) correction.

2.2 The ABEEM/MM potential model for H_2O_2–H_2O system

Based on the previous researchers of our group [49,59], the ABEEM/MM potential energy, $E_{\mathrm{ABEEM/MM}}$, of H_2O_2–H_2O system is expressed as a sum of terms (Eq. (1)), each describing the energy required for distorting a molecule in a specific fashion (Eqs. (2)–(6)).

$$E_{\mathrm{ABEEM/MM}} = E_{\mathrm{str}} + E_{\mathrm{bend}} + E_{\mathrm{tors}} + E_{\mathrm{vdw}} + E_{\mathrm{ele}} \tag{1}$$

$$E_{\mathrm{str}} = \sum_{\mathrm{bonds}} k_r (r - r_{eq})^2 \tag{2}$$

$$E_{\mathrm{bend}} = \sum_{\mathrm{angles}} k_\theta (\theta - \theta_{eq})^2 \tag{3}$$

$$E_{\mathrm{tors}} = \frac{1}{2} \sum_{\mathrm{torsions}} [\nu_1 (1 + \cos\ \varphi) + \nu_2 (1 - \cos\ 2\varphi) + \nu_3 (1 + \cos\ 3\varphi)] \tag{4}$$

$$E_{\mathrm{vdw}} = \sum_{i,j} \left[4 f_{ij} \varepsilon_{ij} \left(\frac{\sigma_{ij}^{12}}{R_{ij}^{12}} - \frac{\sigma_{ij}^{6}}{R_{ij}^{6}} \right) \right] \tag{5}$$

$$\begin{aligned} E_{\mathrm{ele}} = & \sum_i \sum_{j \neq i} \left\{ \sum_{\substack{H \in i \\ (H, lp \text{ in HBIR})}} \sum_{lp \in j} k_{lp,H}(R_{iH,j(lp)}) \frac{q_{iH} q_{j(lp)}}{R_{iH,j(lp)}} \right. \\ & + k \left[\frac{1}{2} \sum_a \sum_b \frac{q_{ia} q_{jb}}{R_{ia,jb}} + \frac{1}{2} \sum_{a-b} \sum_{g-h} \frac{q_{i(a-b)} q_{j(g-h)}}{R_{i(a-b),j(g-h)}} \right. \\ & + \frac{1}{2} \sum_{lp} \sum_{lp'} \frac{q_{i(lp)} q_{j(lp')}}{R_{i(lp),j(lp')}} + \sum_{g-h} \sum_a \frac{q_{ia} q_{j(g-h)}}{R_{ia,j(g-h)}} \\ & \left. \left. + \sum_{\substack{a \\ (a \neq H,\ H \text{ in HBIR} \\ \text{and } lp \text{ not in HBIR})}} \sum_{lp} \frac{q_{ia} q_{j(lp)}}{R_{ia,j(lp)}} + \sum_{lp} \sum_{a-b} \frac{q_{i(a-b)} q_{j(lp)}}{R_{i(a-b),j(lp)}} \right] \right\} \end{aligned} \tag{6}$$

In Eqs. (1) –(6), E_{str} is the energy function for stretching O–O bond or O–H bond in H_2O_2 molecule or H_2O molecule, E_{bend} represents the energy required for bending an angle, E_{tors} is the torsional energy for rotation around O–O bond in H_2O_2 molecule. E_{vdw} and E_{ele} describe the non-bonded atom-atom interactions. k_r, k_θ, ν_1, ν_2 and ν_3 represent the force constants of the bond stretching, angle bending, and dihedral angle torsion, respectively. r_{eq} and θ_{eq} are used to denote the equilibrium values of the bond lengths and angles, respectively. r, θ, and φ stand for the real bond lengths, bond angles, and dihedral angles, respectively. We use Lennard-Jones function to describe the van der Waals energy. The combining rules for the Lennard-Jones coefficients are employed: $\sigma_{ij} = (\sigma_{ii}\sigma_{jj})^{1/2}$ and $\varepsilon_{ij} = (\varepsilon_{ii}\varepsilon_{jj})^{1/2}$. Furthermore, if i and j are intramolecular atoms, the coefficient $f_{ij} = 0.0$ for any i–j pair connected by a valence bond (1–2 pairs) or a valence bond angle (1–3 pairs), $f_{ij} = 0.5$ for 1, 4 interactions (atoms separated by three bonds), and $f_{ij} = 1.0$ for intermolecular cases. For the Coulomb term, q_i and q_j denote the site charges

of atoms, bonds, and lone-pairs, which are obtained by the ABEEM method. R_{ij} is the distance between the site points i and j, and k_{ij} is equal to 0.57 [62], which is an overall optimized correction coefficient in ABEEM. As is known, there are two types of hydrogen bonds between HP and water molecules: The first is that formed between the lone-pair electron on HP oxygen and the water hydrogen (*lp*O(HP)…H–O(water)); the second is formed between the lone-pair electron on water oxygen and HP hydrogen (*lp*O(water)…H–O(HP)). To well depict the nature of the two types of hydrogen bonds, we take special treatment by introducing the parameters $k_{lp\mathrm{O,Hw}}(R_{ij})$ and $k_{lp\mathrm{Ow,H}}(R_{ij})$ to describe the electrostatic interaction of the two types of hydrogen bonds. The fitted expressions of $k_{lp\mathrm{O,Hw}}(R_{ij})$ and $k_{lp\mathrm{Ow,H}}(R_{ij})$ are expressed as follows:

$$k_{lp\mathrm{O,Hw}}(R_{ij}) = 0.660 - \frac{0.140}{1 + \mathrm{e}^{[(R_{ij} - 1.288)/0.022]}}, \quad (7)$$

$$k_{lp\mathrm{Ow,H}}(R_{ij}) = 0.600 - \frac{0.126}{1 + \mathrm{e}^{[(R_{ij} - 1.112)/0.097]}}. \quad (8)$$

The corresponding plots of $k_{lp\mathrm{Ow,H}}(R_{ij})$ and $k_{lp\mathrm{O,Hw}}(R_{ij})$ are shown in Fig. 1. The parameters of HP and water employed here are all taken from Refs. [49,59].

2.3 Molecular dynamics simulations for H_2O_2 aqueous solution

A classical molecular dynamics (MD) simulation was performed in terms of the ABEEM/MM, starting with 70 HP molecules in a cubic box of length 24.662 Å containing 311 H_2O molecules (the mass fraction of HP is about 30%). The system was optimized first, and then the MD simulation was carried out in the isothermal-isobaric (constant pressure and temperature, NPT) ensemble with Anderson thermostats and velocity Verlet integrator. Furthermore, cubic periodic boundary conditions and a time step of 1fs were used, with all bonds to hydrogen constrained using the rattle algorithm. Minimum image conditions were used and no dielectric constant was needed because the explicitly solvent molecules were presented. For molecular dynamics simulation, 0.5 ns of a MD run for equilibration was performed, followed by 1.5 ns of simulations for the calculation of various properties. We recomputed the partial charges of all sites using the ABEEM method every step. Charges are allowed to transfer just between charged sites on the same molecule, not between different molecules. The cutoff radius of 9.0 Å with the nearest image convention is used for the nonbonded interactions in the simulations. The nonbonded interactions are truncated, using force shifting [63], where the calculated forces and energies are smoothly shifted to zero at the cutoff distance.

3 Results and discussion

3.1 Properties of H_2O_2–H_2O dimer

3.1.1 Optimized geometries and interaction energies

Figure 2 depicts the two stable structures of H_2O_2–H_2O dimer, denoted as W1-A and W1-B, respectively. The ABEEM/MM optimized H-bond lengths (Å) are shown first followed by the MP2/aug-cc-pVDZ normal and counterpoise corrections (CP) optimized results. It can be seen from Fig. 2 that the optimized H-bond lengths of MP2 method with CP corrections are obviously longer than those of the MP2 normal optimized results. However, the MP2 CP optimized angles are consistent with those of the MP2 normal optimized results. W1-A has a H-bond structure of five-membered ring, in which the H-bond length of H-Ow is 0.294 Å shorter than that of O-Hw by

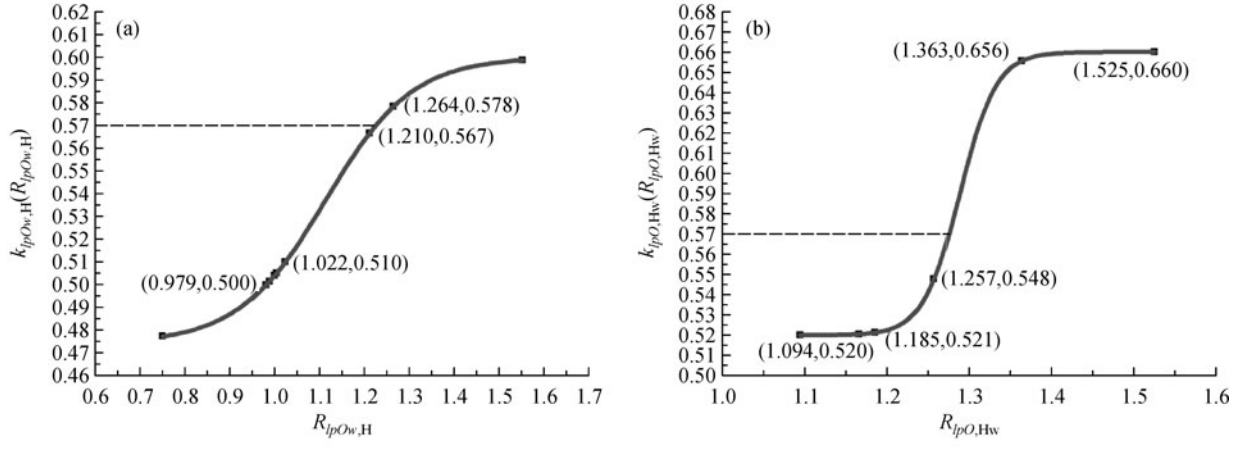

Figure 1 The fitted hydrogen bond functions $k_{lp\mathrm{Ow,H}}(R_{ij})$ and $k_{lp\mathrm{O,Hw}}(R_{ij})$. The fitted data are in parentheses.

ABEEM/MM model (both of the MP2 values are 0.274 Å). W1-B is of a single hydrogen-bonded structure, with one hydrogen atom of H_2O as the proton donor and one oxygen atom of HP as the proton acceptor. And the H-bond length calculated by ABEEM/MM model is 2.013 Å, which is close to the MP2 results of 2.004 Å. In addition, the related angles from ABEEM/MM shown in Fig. 2 agree well with those of MP2 calculations.

The interaction energies of H_2O_2–H_2O dimer calculated by ABEEM/MM model and *ab initio* methods are listed in Table 1. We have taken into account that the correction of the BSSE for the interaction energy should be performed at the BSSE corrected equilibrium geometry. We can see that the interaction energies for the CP and normal optimized geometries are similar. The results have shown that the five-membered ring H-bonded structure (W1-A) is more stable than the single H-bonded structure (W1-B) by 3.26 kcal/mol from ABEEM/MM model, which is close to those of the MP2 calculations (2.92/2.88 kcal/mol). Compared with the MP2 results of this work, the average absolute deviations (AAD) of the ABEEM/MM interaction energies for H_2O_2–H_2O dimer are only 0.17/0.19 kcal/mol.

3.1.2 The ABEEM charge distributions

The ABEEM charge distributions of isolated H_2O_2, H_2O, and H_2O_2–H_2O dimer are listed in Table 2. It is shown that the charge distribution of H_2O_2–H_2O dimer is quite different from those of isolated H_2O and H_2O_2. Two points should be mentioned here: (1) The significant variation of charges takes place at the position where the H-bond forms. There are two types of hydrogen bond formed in W1-A. One is formed between H2 of H_2O_2 and *lp*O5 of H_2O, where q_{H2} increases by 0.0300 while q_{lpOw5} decreases by 0.0581 compared with the isolated H_2O_2 and H_2O. The other is formed between H7 of H_2O and *lp*O3 of H_2O_2, where q_{Hw7} increases by 0.065 while q_{lpO3} decreases by 0.0163 compared with the isolated H_2O and H_2O_2. For W1-B, the obvious charge variations take place at H6 and *lpO1*', where q_{Hw6} increases by 0.0617 and $q_{lpO1'}$ decreases by 0.0047 compared with the isolated H_2O and H_2O_2. (2) As revealed by experimental gas phase data [64] and molecular dynamic simulations of H_2O_2 in aqueous solution [24,64], H_2O_2 is a better proton donor but a poor proton acceptor than H_2O. This can also be confirmed by the analysis of the charge distribution in H_2O_2. From the two parts of H_2O_2 formed H-bond with H_2O, we can easily find that the variation of the lone-pair electronic charges are relatively smaller compared with the charge changes of hydrogen atom. To summarize, the fluctuating charges ABEEM/MM model can reasonably reflect the variations of charge distribution caused by the changing environment.

3.2 Properties of $H_2O_2(H_2O)_n$ (n = 2–6) clusters

3.2.1 Optimized geometries and interaction energies

The ABEEM/MM optimized geometries of hydrated clusters

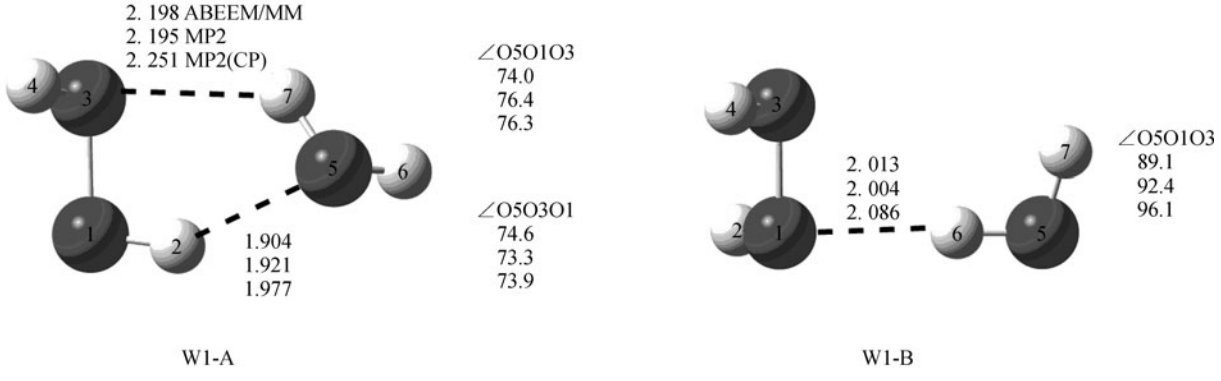

Figure 2 The optimized geometries of H_2O_2–H_2O dimers by ABEEM/MM model, MP2/aug-cc-pVDZ, and MP2/aug-cc-pVDZ (CP) methods. All distances are in Å and angles are in degrees units.

Table 1 Interaction energies of H_2O_2–H_2O dimer (kcal/mol)

	ABEEM/MM	MP2[a)]	MP2[b)]	MP2[c)]	AD[d)]
W1-A	−6.95	−6.78	−6.77	−6.397	0.17/0.18
W1-B	−3.69	−3.86	−3.89	−3.689	0.17/0.20

(a) MP2/aug-cc-pVTZ//MP2/aug-cc-pVDZ with BSSE correction in this work;
(b) MP2/aug-cc-pVTZ//MP2/aug-cc-pVDZ (with CP optimized) with BSSE correction in this work;
(c) MP2/6-311 ++ G(2d,2p)(6d, 10f)//MP2/6-311 ++ G(2d,2p)(6d, 10f) with BSSE correction from Ref. [14];
(d) Absolute deviation (AD) is the ABEEM/MM result with respect to those of MP2[a)] and MP2[b)] calculations

Table 2 ABEEM charge distributions of complexes W1-A and W1-B, isolated H_2O_2 and H_2O

	W1-A	CC[a)]	W1-B	CC[a)]	Isolated H_2O_2	
q_{O1}	0.0241	−0.0006	0.0244	−0.0003	q_{O1}/q_{O3}	0.0247
q_{H2}	**0.3695**	**0.0300**	0.3451	0.0056	q_{H2}/q_{H4}	0.3395
q_{O3}	0.0230	−0.0017	0.0245	−0.0002	$q_{O1\text{-}O3}$	−0.0361
q_{H4}	0.3322	−0.0073	0.3449	0.0054	$q_{O1\text{-}H2}/q_{O3\text{-}H4}$	−0.0416
q_{Ow5}	0.1009	−0.0116	0.0973	−0.0152	q_{lpO1}/q_{lpO3}	−0.1548
q_{Hw6}	0.2898	0.0001	**0.3514**	**0.0617**	$q_{lpO1'}/q_{lpO3'}$	−0.1498
q_{Hw7}	**0.3547**	**0.0650**	0.2593	−0.0304	Isolated H_2O	
$q_{O1\text{-}H2}$	−0.0432	−0.0016	−0.0418	−0.0002	q_{O1}	0.1125
$q_{O1\text{-}O3}$	−0.0379	−0.0018	−0.0374	−0.0013	q_{H2}/q_{H3}	0.2897
$q_{O3\text{-}H4}$	−0.0415	0.0001	−0.0418	−0.0002	$q_{O1\text{-}H2}/q_{O1\text{-}H3}$	−0.1552
$q_{Ow5\text{-}Hw6}$	−0.1486	0.0066	−0.1460	0.0092	$q_{lpO1}/q_{lpO1'}$	−0.1908
$q_{Ow5\text{-}Hw7}$	−0.1468	0.0084	−0.1492	0.0060		
q_{lpO1}	−0.1512	0.0036	−0.1537	−0.0039		
$q_{lpO1'}$	−0.1556	−0.0058	**−0.1595**	**−0.0047**		
q_{lpO3}	**−0.1661**	**−0.0163**	−0.1511	0.0037		
$q_{lpO3'}$	−0.1532	0.0016	−0.1537	−0.0039		
q_{lpOw5}	**−0.2489**	**−0.0581**	−0.2056	−0.0148		
$q_{lpOw5'}$	−0.2011	−0.0103	−0.2072	−0.0164		

a) Variations of the charges compared with the isolated H_2O_2 and H_2O

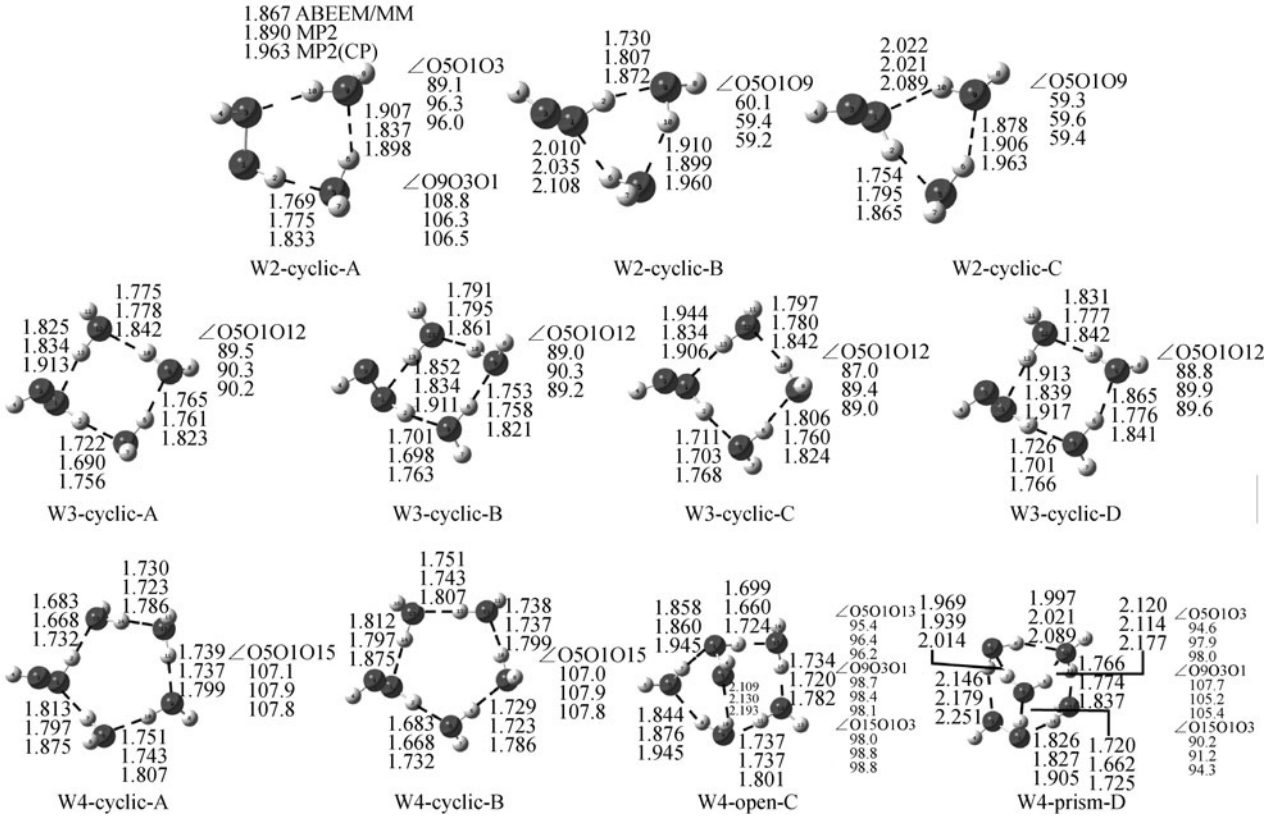

Figure 3 The optimized geometries of $H_2O_2(H_2O)_{2-4}$ clusters by ABEEM/MM model, MP2/aug-cc-pVDZ, and MP2/aug-cc-pVDZ (CP) methods. All distances are in Å and angles are in degrees units.

of $H_2O_2(H_2O)_n$ (n = 2–6) are presented in Figs. 3 and 4, along with the corresponding H-bond lengths (Å). The corresponding interaction energies of these structures determined by ABEEM/MM model and several *ab initio* methods are listed in Table 3. For n = 2, three cyclic H-bond structures are obtained by ABEEM/MM model. The seven-membered ring

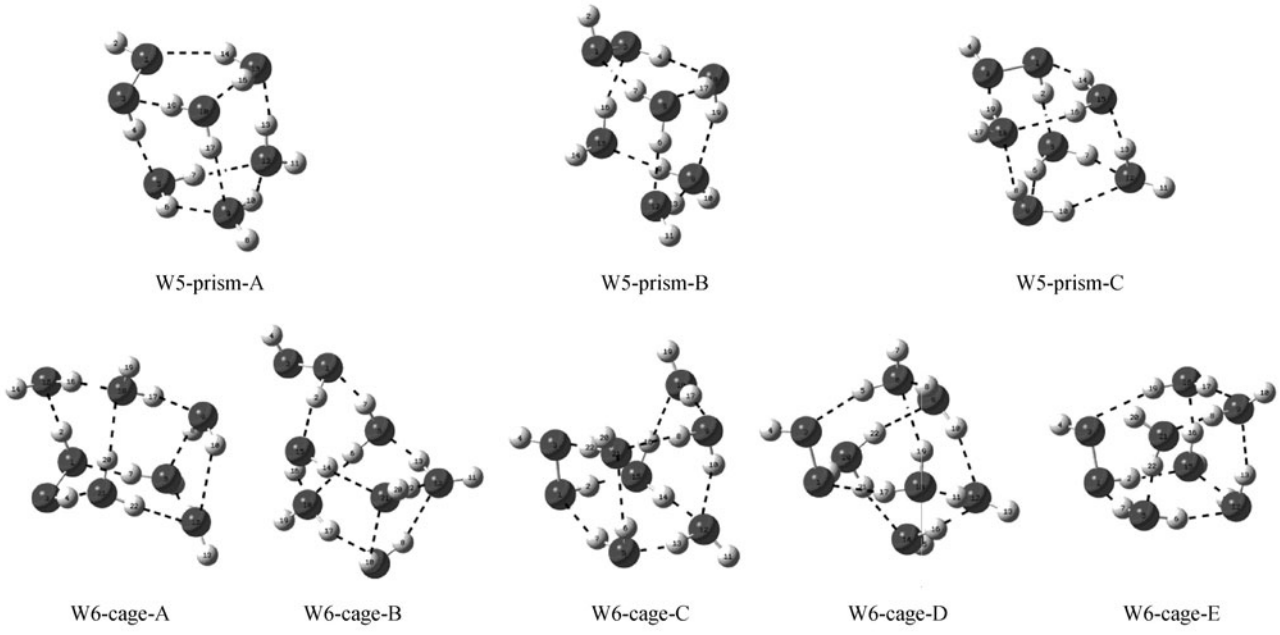

Figure 4 The optimized geometries of $H_2O_2(H_2O)_{5,6}$ clusters by ABEEM/MM model, MP2/aug-cc-pVDZ, and MP2/aug-cc-pVDZ (CP) methods.

Table 3 Interaction energies of $H_2O_2(H_2O)_n$ (n = 2–6) clusters (kcal/mol)

	ABEEM/MM	MP2[a)]	MP2[b)]	MP2[c)]	AD[d)]
W2-cyclic-A	−16.91	−16.71	−16.65	−15.813	0.20/0.26
W2-cyclic-B	−15.81	−15.35	−15.31	−14.614	0.46/0.50
W2-cyclic-C	−15.49	−15.22	−15.24	−14.602	0.27/0.25
W3-cyclic-A	−27.69	−26.78	−26.72	−25.709	0.91/0.97
W3-cyclic-B	−27.36	−26.17	−26.10	−25.126	1.19/1.26
W3-cyclic-C	−26.14	−26.09	−26.07	−25.063	0.05/0.07
W3-cyclic-D	−26.36	−26.09	−26.02		0.27/0.34
W4-cyclic-A	−36.02	−35.59	−35.48	−34.212	0.43/0.54
W4-cyclic-B	−36.04	−35.59	−35.48	−34.207	0.45/0.56
W4-open-C	−35.21	−35.48	−35.35	−34.058	0.27/0.14
W4-prism-D	−33.41	−34.60	−34.49		1.18/1.08
W5-prism-A	−50.99	−45.53	−45.36	−43.651	5.46/5.63
W5-prism-B	−46.61	−44.69	−44.59	−42.841	1.92/2.02
W5-prism-C	−46.43	−44.60	−44.48	−42.748	1.83/1.95
W6-cage-A	−55.86	−56.48	−56.29	−55.183	0.62/0.43
W6-cage-B	−53.56	−55.23	−55.07		1.67/1.51
W6-cage-C	−55.68	−54.89	−54.75		0.79/0.93
W6-cage-D	−54.44	−54.88	−54.69		0.44/0.25
W6-cage-E	−51.59	−54.72	−54.58		3.13/2.99

a) MP2/aug-cc-pVTZ//MP2/aug-cc-pVDZ with BSSE correction in this work;
b) MP2/aug-cc-pVTZ//MP2/aug-cc-pVDZ(CP optimized) with BSSE correction in this work;
c) MP2/6-311 ++ G(2d,2p)(6d,10f)//MP2/6-311 ++ G(2d,2p)(6d,10f) with BSSE correction from Ref. [14];
d) Absolute deviation (AD) is the ABEEM/MM result with respect to those of MP2[a)] and MP2[b)] calculations.

structure, named W2-cyclic-A, which can be viewed as a combination of water dimer with an HP molecule linked by hydrogen bonds, and this is more energy favorable than the other two six-membered ring hydrogen bond structures (W2-cyclic-B and W2-cyclic-C). The interaction energies calculated by ABEEM/MM model for 1∶2 complexes are −16.91, −15.81 and −15.49 kcal/mol, respectively, which agree well with those of MP2/aug-cc-pVTZ//MP2/aug-cc-pVDZ results.

For n = 3, all four structures are energetically close to each other, and W3-cyclic-A is the most stable structure indicated by ABEEM/MM model and MP2 methods. The energy order of these conformations is W3-cyclic-A < W3-cyclic-B < W3-cyclic-D < W3-cyclic-C, and the interaction energies from the ABEEM/MM model are close to those from the MP2 calculation. W3-cyclic-A has the smallest ABEEM/MM interaction energy of −27.69 kcal/mol (MP2 value is −26.78/−26.72 kcal/mol), and W3-cyclic-C has the greatest ABEEM/MM interaction energy of −26.14 kcal/mol (W3-cyclic-C and W3-cyclic-D have the same interaction energies of −26.09 kcal/mol at MP2 level, and MP2(CP) values are −26.07 and −26.02 kcal/mol, respectively).

For n = 4, the four stable structures are portrayed in Fig. 3, from which the obvious transformation from 2D planar structure to 3D hydrogen bonding network structure can be seen. The cyclic structures (W4-cyclic-A and W4-cyclic-B) are relatively more stable than the open structure (W4-open-C) and the prism structure (W4-prism-D) both from ABEEM/MM model and MP2 methods. The interaction energies calculated by ABEEM/MM model for n = 4 are −36.02, −36.04, −35.21 and −33.41 kcal/mol, respectively, which is in accordance with the MP2 calculations of −35.59/−35.48, −35.59/−35.48, −35.48/−35.35 and −34.60/−34.49 kcal/mol.

For n = 5, three prism-like structures are shown in Fig. 4. The interaction energies calculated by ABEEM/MM model are −50.99, −46.61 and −46.43 kcal/mol, respectively. Although ABEEM/MM model overestimates the interaction energy of W5-prism-A, it is acceptable as the deviations of the interaction energies for the other two structures relative to MP2 results are all within 2 kcal/mol, and the energy order is consistent with those from MP2 method. For n = 6, five of the most favorable clusters, namely, W6-cage-A, W6-cage-B, W6-cage-C, W6-cage-D, and W6-cage-E, are shown in Fig. 4, where the increased number of H-bonds is evident. The interaction energy of the most possible structure, W6-cage-A is −55.86 kcal/mol, which is also in accordance with the MP2 results (−56.48/−56.29 kcal/mol). For the other four complexes, the maximum deviation with respect to MP2 results is within 6%.

The changing tendencies of the average H-bond lengths for O-Hw and H-Ow in the hydrated clusters of $HP(H_2O)_n$ (n = 1–6) are depicted in Fig. 5. From the viewpoint of geometrical structure, three points must be mentioned: (1) From n = 1 to 4, in the wake of the augmentation of the cyclic structure, all the H-bond lengths are shortened obviously. This trend can be clearly seen in Fig. 5. (2) n = 4 is the transition state structure from 2D planar structure to 3D network structure. From the cyclic structure to open structure, the H-bond length of O-Hw is elongated by about 0.171 Å by ABEEM/MM model, close to the MP2 results of 0.198/0.194 Å. But from open structure to prism structure, the H-bond length of O-Hw changes inconspicuously. However, the H-bond length of H-Ow remains steady along with the transformation from cyclic structure to prism structure for n = 4. (3) From n = 5 to 6, the ABEEM/MM H-bond lengths of O-Hw decreases about 0.078 Å, which is consistent with the MP2/aug-cc-pVDZ

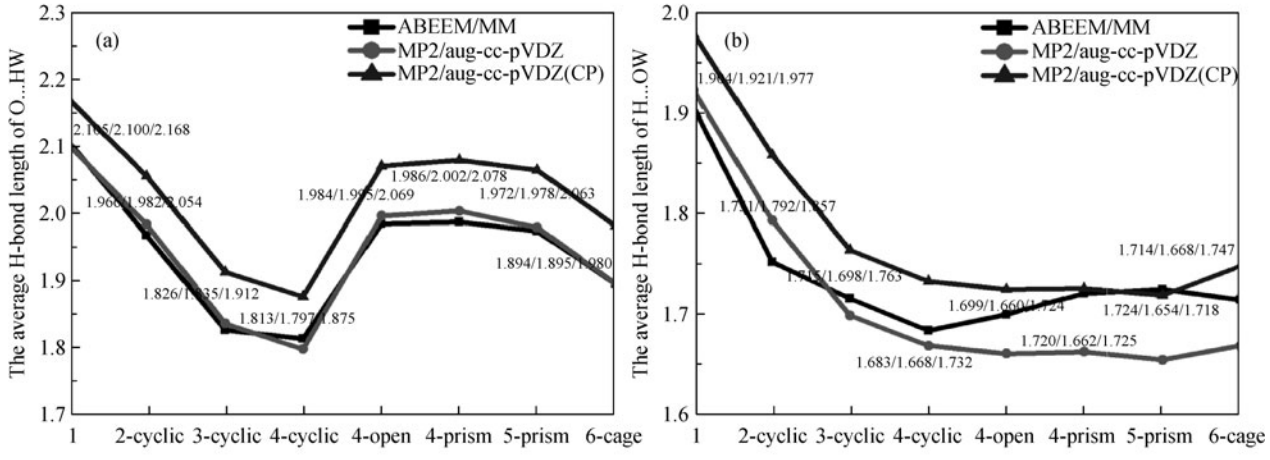

Figure 5 Variation of the average H-bond length with the increasing number of water molecules. (a) O-Hw (b) H-Ow. All distances are in Å units.

results (0.083 Å). However, the ABEEM/MM H-bond length of H-Ow decreases 0.010 Å from n = 5 to n = 6, while the MP2 results increases by 0.014/0.029 Å.

In summary, from n = 1 to 6, the overall trends of the interaction energy of $HP(H_2O)_n$ (n = 1–6) is that it increases about 10 kcal/mol, which is about twice as the interaction energy of water dimer when a water molecule is added. The MP2 CP optimized H-bond lengths are obviously longer than those of the normal MP2 optimized and ABEEM/MM results, and the average value is about 0.070 Å. However, the interaction energies between the CP and normal optimized geometries are negligible. Compared with MP2/aug-cc-pVTZ//MP2/aug-cc-pVDZ method, ABEEM fluctuating charge potential model can give correct description of the geometries and interaction energies of $H_2O_2(H_2O)_n$ (n = 1–6). The AAD for interaction energies is 1.00 kcal/mol, and the AAD of H-bond lengths and angles associated with the HP molecule (shown in Fig. 4, but not shown in Fig. 5 for clarity) are 0.024 Å and 1.8°, respectively.

3.2.2 Dipole moments

The charge distribution of $H_2O_2(H_2O)_n$ (n = 2–6) complexes are listed in supplementary materials. Similar to the H_2O_2–H_2O dimer, the variation of charge in the $H_2O_2(H_2O)_n$ (n = 2–6) clusters are mainly at the positions where H-bonds form. Dipole moment is an important quality for representing charge distributions, which can be the criterion of reasonable charge distribution. In addition, it can provide the total information of structural properties. Correlation of the dipoles for $H_2O_2(H_2O)_n$ (n = 1–6) evaluated with *ab initio* calculations at MP2/aug-cc-pVTZ level and the ABEEM/MM model is shown in Fig. 6, and the linear correlation coefficient is 0.9498. This further validates the reliability of the newly constructed ABEEM/MM interaction potential for H_2O_2–H_2O systems.

3.3 Structural properties of H_2O_2 in aqueous solution

The detailed structure of H_2O_2 in aqueous solution is characterized by the radial distribution functions (RDFs), which describes how the density of surrounding atoms varies as a function of the distance from a particular atom. Here, the structure feature of the water molecules surrounding the HP is described by the RDFs of the hydrogen atoms of water molecules around the oxygen atom of HP (Fig. 7(a)) and the oxygen atoms of water molecules around the hydrogen atom on the HP (Fig. 7(b)). The $g_{O\text{-}Hw}$ shows a sharp and low first peak located at 2.019 Å, followed by a higher second peak centered at about 3.250 Å, and the third peak is very weak located at about 6.0 Å. The $g_{H\text{-}Ow}$ has a high and sharp first peak located at 1.749 Å corresponding to the first hydration shell, followed by a lower and boarder second peak centered at about 3.675 Å. The $g_{H\text{-}Ow}$ has well-defined first peaks, indicating strong hydrogen bond interaction between the hydrogen on the HP and water oxygen. Meanwhile, the first peak of $g_{H\text{-}Ow}$ is about 0.270 Å shorter than that of $g_{O\text{-}Hw}$, and this also shows that the HP is a good proton donor and poor proton acceptor in aqueous solution.

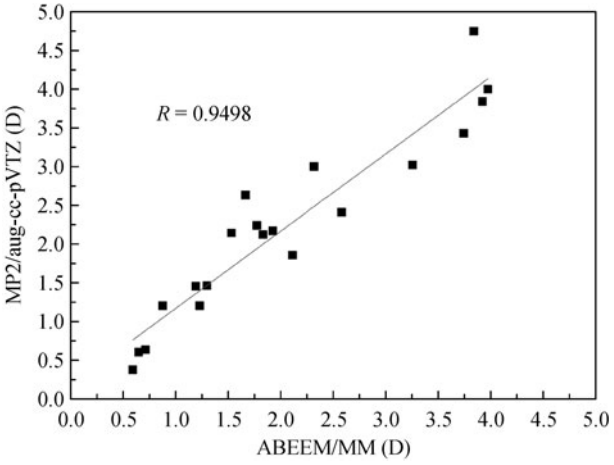

Figure 6 Correlation of dipole moments of $H_2O_2(H_2O)_n$ (n = 1–6) clusters between *ab initio* and ABEEM/MM model.

4 Conclusion and outlook

In this work, we have systematically investigated the hydrogen bond interaction between HP and water (with up to six water molecules) by high-level *ab initio* method and a newly constructed ABEEM/MM fluctuating charge model. This potential gives reasonable properties of H_2O_2–H_2O clusters through comparision with the *ab initio* calculations. The AAD for interaction energies, H-bond lengths and angles associated with HP are 1.00 kcal/mol, 0.024 Å and 1.8°, respectively. The linear correlation coefficient of dipole moments between ABEEM/MM model and MP2/aug-cc-pVDZ method reaches 0.9498. The ABEEM/MM results also indicate that n = 4 is the transition state structure from 2D planar structure to 3D network structure. The variation of the average H-bond length with the increasing number of water molecules given by ABEEM/MM model agree well with those given by the *ab initio* studies. Molecular dynamics simulation HP aqueous solution has been carried out by ABEEM/MM model, and the results confirms that HP is a good proton donor and poor proton acceptor in aqueous solution through the analysis of the RDFs and the charge distributions.

Overall, the newly constructed ABEEM potential model

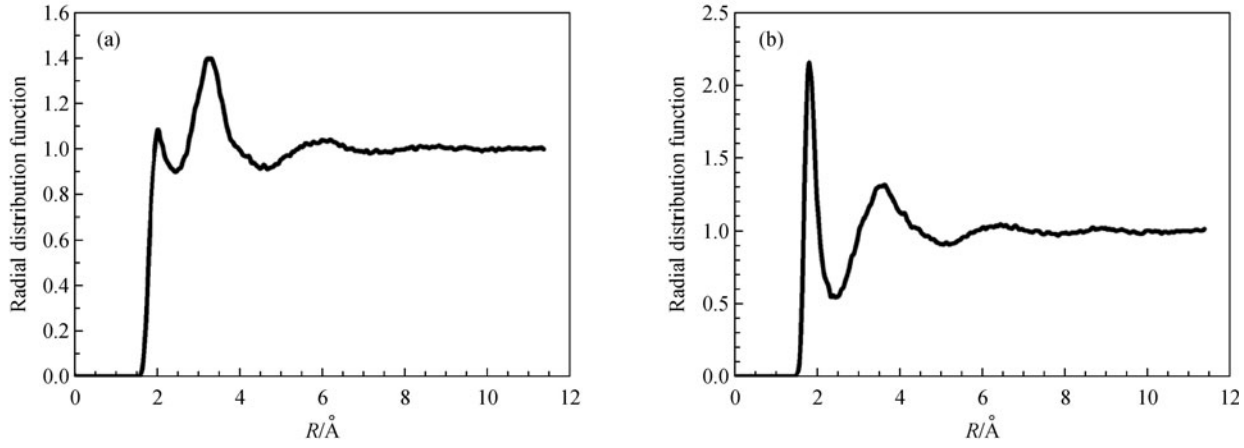

Figure 7 Radial distribution functions at 298.15 K for the HP aqueous solution by ABEEM/MM/MD model. (a) $g_{O\text{-}Hw}$; (b) $g_{H\text{-}Ow}$

can reproduce rather accurate structural and energetic properties of $H_2O_2(H_2O)_n$ (n = 1–6) clusters and H_2O_2 aqueous solution. Based on this potential, studies of H_2O_2 interaction with nucleic acid base in aqueous solution has been undertaking.

Acknowledgements The authors greatly thank Professor Jay William Ponder for providing the Tinker programs. This work was supported by the grant from the National Natural Science Foundation of China (Nos. 21133005 and 20703022) and the Foundation of Education Bureau of Liaoning Province of China (No. 2009T057).

Supplementary materials

Table S1 The charge distribution of $H_2O_2(H_2O)_2$

	W2-cyclic-A	W2-cyclic-B	W2-cyclic-C		W2-cyclic-A	W2-cyclic-B	W2-cyclic-C
q_{O1}	0.0242	0.0233	0.0231	$q_{Ow5\text{-}Hw6}$	−0.1452	−0.1464	−0.1452
q_{H2}	**0.3801**	**0.3758**	**0.3749**	$q_{Ow5\text{-}Hw7}$	−0.1508	−0.1496	−0.1510
q_{O3}	0.0214	0.0227	0.0232	$q_{Ow8\text{-}Hw9}$	−0.1501	−0.1506	−0.1495
q_{H4}	0.3314	0.3326	0.3325	$q_{Ow8\text{-}Hw10}$	−0.1462	−0.1451	−0.1462
q_{Ow5}	0.1024	0.1032	0.1020	q_{lpO1}	−0.1513	−0.1556	**−0.1636**
q_{Hw6}	**0.4116**	**0.3805**	**0.4083**	$q_{lpO1'}$	−0.1552	**−0.1621**	−0.1561
q_{Hw7}	0.2667	0.2871	0.2646	q_{lpO3}	**−0.1691**	−0.1554	−0.1559
q_{Ow8}	0.1034	0.1017	0.1028	$q_{lpO3'}$	−0.1577	−0.1563	−0.1539
q_{Hw9}	0.2799	0.2673	0.2846	q_{lpOw5}	**−0.2649**	−0.2034	**−0.2678**
q_{Hw10}	**0.3908**	**0.4082**	**0.3822**	$q_{lpOw5'}$	−0.2198	**−0.2714**	−0.2109
$q_{O1\text{-}H2}$	−0.0434	−0.0430	−0.0430	q_{lpOw8}	**−0.2696**	−0.2157	**−0.2665**
$q_{O1\text{-}O3}$	−0.0388	−0.0404	−0.0397	$q_{lpOw8'}$	−0.2081	**−0.2658**	−0.2073
$q_{O3\text{-}H4}$	−0.0419	−0.0415	−0.0415				

Table S2 The charge distribution of $H_2O_2(H_2O)_3$

	W3-cyclic-A	W3-cyclic-B	W3-cyclic-C	W3-cyclic-D
q_{O1}	0.0219	0.0220	0.0227	0.0229
q_{H2}	**0.3806**	**0.3797**	**0.3817**	**0.3825**
q_{O3}	0.0225	0.0225	0.0228	0.0223
q_{H4}	0.3306	0.3308	0.3318	0.3325
q_{Ow5}	0.1032	0.1032	0.1027	0.1029
q_{Hw6}	**0.4479**	**0.4481**	**0.4315**	**0.4222**
q_{Hw7}	0.2459	0.2472	0.2567	0.2651
q_{Ow8}	0.1066	0.1065	0.1048	0.1044
q_{Hw9}	0.2624	0.2631	0.2624	0.2617
q_{Hw10}	**0.4496**	**0.4485**	**0.4288**	**0.4283**
q_{Ow11}	0.1047	0.1046	0.1038	0.1042
q_{Hw12}	0.2989	0.2972	0.2810	0.2819
q_{Hw13}	**0.3882**	**0.3878**	**0.4022**	**0.4019**
$q_{O1\text{-}H2}$	−0.0432	−0.0431	−0.0435	−0.0435
$q_{O1\text{-}O3}$	−0.0418	−0.0419	−0.0411	−0.0418
$q_{O3\text{-}H4}$	−0.0416	−0.0416	−0.0416	−0.0417
$q_{Ow5\text{-}Hw6}$	−0.1437	−0.1438	−0.1437	−0.1449
$q_{Ow5\text{-}Hw7}$	−0.1529	−0.1527	−0.1518	−0.1512
$q_{Ow8\text{-}Hw9}$	−0.1526	−0.1525	−0.1521	−0.1518
$q_{Ow8\text{-}Hw10}$	−0.1444	−0.1446	−0.1451	−0.1444
$q_{Ow11\text{-}Hw12}$	−0.1493	−0.1493	−0.1502	−0.1504
$q_{Ow11\text{-}Hw13}$	−0.1443	−0.1444	−0.1455	−0.1459
q_{lpO1}	**−0.1599**	**−0.1599**	**−0.1655**	**−0.1645**
$q_{lpO1'}$	−0.1568	−0.1568	−0.1565	−0.1557
q_{lpO3}	−0.1561	−0.1558	−0.1555	−0.1560
$q_{lpO3'}$	−0.1563	−0.1562	−0.1554	−0.1571
q_{lpOw5}	**−0.2788**	−0.2244	−0.2250	−0.2273
$q_{lpOw5'}$	−0.2216	**−0.2775**	**−0.2704**	**−0.2668**
q_{lpOw8}	**−0.2895**	−0.2328	−0.2146	**−0.2771**
$q_{lpOw8'}$	−0.2320	**−0.2883**	**−0.2843**	−0.2212
q_{lpOw11}	−0.2180	−0.2187	**−0.2684**	−0.2142
$q_{lpOw11'}$	**−0.2802**	**−0.2772**	−0.2228	**−0.2776**

Table S3 The charge distribution of $H_2O_2(H_2O)_4$

	W4-cyclic-A	W4-cyclic-B	W4-open-C	W4-prism-D
q_{O1}	0.0216	0.0216	0.0220	0.0222
q_{H2}	**0.3817**	**0.3817**	**0.3827**	**0.3843**
q_{O3}	0.0224	0.0224	0.0220	0.0223
q_{H4}	0.3320	0.3321	0.3328	0.3340
q_{Ow5}	0.1036	0.1030	0.1018	0.1046
q_{Hw6}	0.2972	**0.4468**	0.2905	**0.3426**
q_{Hw7}	**0.3859**	0.2483	**0.3670**	**0.3658**
q_{Ow8}	0.1050	0.1053	0.1061	0.1033
q_{Hw9}	0.2620	0.2592	**0.4090**	**0.3590**
q_{Hw10}	**0.4435**	**0.4485**	**0.3048**	**0.3140**
q_{Ow11}	0.1053	0.1050	0.1051	0.1069
q_{Hw12}	**0.4484**	0.2619	**0.4573**	0.2754
q_{Hw13}	0.2593	**0.4436**	0.2525	**0.4323**
q_{Ow14}	0.1030	0.1036	0.1033	0.1027
q_{Hw15}	**0.4468**	**0.3858**	0.2498	**0.3800**
q_{Hw16}	0.2483	0.2974	**0.4472**	0.2947

(*Continued*)

	W4-cyclic-A	W4-cyclic-B	W4-open-C	W4-prism-D
$q_{O1\text{-}H2}$	−0.0433	−0.0433	−0.0432	−0.0431
$q_{O1\text{-}O3}$	−0.0425	−0.0425	−0.0415	−0.0414
$q_{O3\text{-}H4}$	−0.0417	−0.0417	−0.0417	−0.0417
$q_{Ow5\text{-}Hw6}$	−0.1493	−0.1429	−0.1487	−0.1500
$q_{Ow5\text{-}Hw7}$	−0.1443	−0.1527	−0.1448	−0.1491
$q_{Ow8\text{-}Hw9}$	−0.1523	−0.1526	−0.1463	−0.1486
$q_{Ow8\text{-}Hw10}$	−0.1435	−0.1434	−0.1507	−0.1506
$q_{Ow11\text{-}Hw12}$	−0.1434	−0.1523	−0.1429	−0.1516
$q_{Ow11\text{-}Hw13}$	−0.1526	−0.1435	−0.1528	−0.1446
$q_{Ow14\text{-}Hw15}$	−0.1429	−0.1443	−0.1526	−0.1444
$q_{Ow14\text{-}Hw16}$	−0.1527	−0.1493	−0.1431	−0.1490
q_{lpO1}	−0.1569	**−0.1611**	−0.1569	**−0.1602**
$q_{lpO1'}$	**−0.1611**	−0.1569	**−0.1610**	−0.1560
q_{lpO3}	−0.1567	−0.1556	−0.1574	**−0.1638**
$q_{lpO3'}$	−0.1556	−0.1567	−0.1577	−0.1565
q_{lpOw5}	**−0.2862**	−0.2216	**−0.2673**	**−0.2903**
$q_{lpOw5'}$	−0.2069	**−0.2809**	−0.1987	−0.2236
q_{lpOw8}	−0.2213	−0.2205	−0.2201	**−0.2647**
$q_{lpOw8'}$	**−0.2933**	**−0.2965**	**−0.3027**	−0.2125
q_{lpOw11}	−0.2205	**−0.2935**	−0.2260	**−0.2579**
$q_{lpOw11'}$	**−0.2964**	−0.2212	**−0.2932**	**−0.2604**
q_{lpOw14}	**−0.2809**	**−0.2863**	−0.2244	**−0.2775**
$q_{lpOw14'}$	−0.2216	−0.2069	**−0.2802**	−0.2066

Table S4 The charge distribution of $H_2O_2(H_2O)_5$

	W5-prism-A	W5-prism-C		W5-prism-A	W5-prism-C
q_{O1}	0.0220	0.0231	$q_{Ow5\text{-}Hw7}$	−0.1470	−0.1485
q_{H2}	0.3314	0.3910	$q_{Ow8\text{-}Hw9}$	−0.1511	−0.1507
q_{O3}	0.0229	0.0211	$q_{Ow8\text{-}Hw10}$	−0.1459	−0.1495
q_{H4}	0.3791	0.3312	$q_{Ow11\text{-}Hw12}$	−0.1543	−0.1500
q_{Ow5}	0.1032	0.1055	$q_{Ow11\text{-}Hw13}$	−0.1433	−0.1521
q_{Hw6}	0.3028	0.3872	$q_{Ow14\text{-}Hw15}$	−0.1516	−0.1444
q_{Hw7}	0.3901	0.3375	$q_{Ow14\text{-}Hw16}$	−0.1456	−0.1486
q_{Ow8}	0.1048	0.1047	$q_{Ow17\text{-}Hw18}$	−0.1475	−0.1480
q_{Hw9}	0.2739	0.3490	$q_{Ow17\text{-}Hw19}$	−0.1500	−0.1502
q_{Hw10}	0.4167	0.3437	q_{lpO1}	−0.1583	−0.1469
q_{Ow11}	0.1114	0.1067	$q_{lpO1'}$	−0.1578	−0.1579
q_{Hw12}	0.2642	0.2672	q_{lpO3}	−0.1585	−0.1555
q_{Hw13}	0.4989	0.4381	$q_{lpO3'}$	−0.1563	−0.1587
q_{Ow14}	0.1084	0.1050	q_{lpOw5}	−0.2203	−0.1693
q_{Hw15}	0.3074	0.3281	$q_{lpOw5'}$	−0.2787	−0.2328
q_{Hw16}	0.4337	0.3744	q_{lpOw8}	−0.2322	−0.2982
q_{Ow17}	0.1050	0.1067	$q_{lpOw8'}$	−0.2661	−0.2171
q_{Hw18}	0.3864	0.2975	q_{lpOw11}	−0.2844	−0.2809
q_{Hw19}	0.3144	0.4017	$q_{lpOw11'}$	−0.2925	−0.2564
$q_{O1\text{-}H2}$	−0.0417	−0.0431	q_{lpOw14}	−0.3295	−0.2590
$q_{O1\text{-}O3}$	−0.0400	−0.0404	$q_{lpOw14'}$	−0.2228	−0.2948
$q_{O3\text{-}H4}$	−0.0430	−0.0416	q_{lpOw17}	−0.2156	−0.2161
$q_{Ow5\text{-}Hw6}$	−0.1500	0.0231	$q_{lpOw17'}$	−0.2926	−0.2577

Table S5 The charge distribution of $H_2O_2(H_2O)_6$

	W6-cage-A	W6-cage-E		W6-cage-A	W6-cage-E
q_{O1}	0.0186	0.0227	$q_{Ow8\text{-}Hw9}$	−0.1469	−0.1504
q_{H2}	0.3630	0.3916	$q_{Ow8\text{-}Hw10}$	−0.1505	−0.1494
q_{O3}	0.0230	0.0206	$q_{Ow11\text{-}Hw12}$	−0.1461	−0.1522
q_{H4}	0.3675	0.3289	$q_{Ow11\text{-}Hw13}$	−0.1504	−0.1445
q_{Ow5}	0.1092	0.1053	$q_{Ow14\text{-}Hw15}$	−0.1513	−0.1513
q_{Hw6}	0.3026	0.3678	$q_{Ow14\text{-}Hw16}$	−0.1444	−0.1484
q_{Hw7}	0.4309	0.3358	$q_{Ow17\text{-}Hw18}$	−0.1438	−0.1437
q_{Ow8}	0.1061	0.1065	$q_{Ow17\text{-}Hw19}$	−0.1532	−0.1521
q_{Hw9}	0.4031	0.3476	$q_{Ow20\text{-}Hw21}$	−0.1496	−0.1489
q_{Hw10}	0.3110	0.3734	$q_{Ow20\text{-}Hw22}$	−0.1496	−0.1456
q_{Ow11}	0.1038	0.1081	q_{lpO1}	−0.1619	−0.1562
q_{Hw12}	0.4015	0.2745	$q_{lpO1'}$	−0.1710	−0.1595
q_{Hw13}	0.2802	0.4466	q_{lpO3}	−0.1564	−0.1643
q_{Ow14}	0.1018	0.1061	$q_{lpO3'}$	−0.1550	−0.1578
q_{Hw15}	0.2610	0.3422	q_{lpOw5}	−0.2772	−0.2985
q_{Hw16}	0.4133	0.3909	$q_{lpOw5'}$	−0.2705	−0.2136
q_{Ow17}	0.1089	0.1038	q_{lpOw8}	−0.2153	−0.3004
q_{Hw18}	0.4652	0.4347	$q_{lpOw8'}$	−0.3076	−0.2273
q_{Hw19}	0.2681	0.2518	q_{lpOw11}	−0.2277	−0.2697
q_{Ow20}	0.1038	0.1056	$q_{lpOw11'}$	−0.2615	−0.2628
q_{Hw21}	0.3511	0.3071	q_{lpOw14}	−0.2661	−0.2387
q_{Hw22}	0.3517	0.3807	$q_{lpOw14'}$	−0.2142	−0.3009
$q_{O1\text{-}H2}$	−0.0427	−0.0431	q_{lpOw17}	−0.2784	−0.2207
$q_{O1\text{-}O3}$	−0.0425	−0.0411	$q_{lpOw17'}$	−0.2667	−0.2738
$q_{O3\text{-}H4}$	−0.0427	−0.0417	q_{lpOw20}	−0.2266	−0.2468
$q_{Ow5\text{-}Hw6}$	−0.1510	−0.1485	$q_{lpOw20'}$	−0.2807	−0.2521
$q_{Ow5\text{-}Hw7}$	−0.1440	−0.1482			

References

1. Baalen, C. V.; Marler, J. E., *Nature* **1966**, *211*, 951
2. Robbinmartin, L.; Damschen, D., *Atmospheric Environment (1967)* **1981**, *15*, 1615–1621
3. Hoffmann, M. R.; Edwards, J. O., *J. Phys. Chem*. **1975**, *79*, 2096–2098
4. McArdle, J. V.; Hoffmann, M. R., *J. Phys. Chem*. **1983**, *87*, 5425–5429
5. Reeves, C. E.; Penkett, S. A., *Chem. Rev*. **2003**, *103*, 5199–5218
6. Pascual, L. M.; Daniele, M. B.; Pájaro, C.; Barberis, L., *Contraception* **2006**, *73*, 78–81
7. Katsinelos, P.; Kountouras, J.; Paroutoglou, G.; Beltsis, A.; Mimidis, K.; Pilpilidis, I.; Zavos, C., *Eur. J. Gastroenterol. Hepatol*. **2006**, *18*, 107–110
8. Shigematsu, M.; Kitajima, M.; Ogawa, K.; Higo, T.; Hotokebuchi, T., *J. Arthroplasty* **2005**, *20*, 639–646
9. Kunen, S. M.; Lazrus, A. L.; Kok, G. L.; Heikes, B. G., *J. Geophys. Res*. **1983**, *88*, 3671–3674
10. McArdle, J. V.; Hoffmann, M. R., *J. Chem. Phys*. **1983**, *87*, 5425–5429
11. Varma, S. D.; Devamanoharan, P. S., *Free Radic. Res. Commun*. **1991**, *14*, 125–131
12. Sennikov, P. G.; Ignatov, S. K.; Schrems, O., *ChemPhysChem* **2005**, *6*, 392–412
13. Du, D.; Fu, A.; Zhou, Z. y., *J. Mol. Struct. THEOCHEM* **2005**, *717*, 127–132
14. Kulkarni, A. D.; Pathak, R. K.; Bartolotti, L. J., *J. Phys. Chem. A* **2005**, *109*, 4583–4590
15. Kulkarni, A. D.; Pathak, R. K.; Bartolotti, L. J., *J. Chem. Phys*. **2006**, *124*, 214309
16. Ju, X. H.; Xiao, J. J.; Xiao, H. M., *J. Mol. Struct. THEOCHEM* **2003**, *626*, 231–238
17. Dobado, J. A.; Molina, J. M., *J. Phys. Chem*. **1994**, *98*, 1819–1825
18. González, L.; Mó, O.; Yáñez, M., *J. Comput. Chem*. **1997**, *18*, 1124–1135
19. Mó, O.; Yáñez, M.; Rozas, I.; Elguero, J., *Chem. Phys. Lett*. **1994**, *219*, 45–52
20. Ferreira, C.; Martiniano, H. F. M. C.; Cabral, B. J. C.; Aquilanti, V., *Int. J. Quantum Chem*. **2011**, *111*, 1824–1835
21. Ignatov, S. K.; Sennikov, P. G.; Jacobi, H. W.; Razuvaev, A. G.; Schrems, O., *Phys. Chem. Chem. Phys*. **2003**, *5*, 496–505
22. Akiya, N.; Savage, P. E., *J. Phys. Chem. A* **2000**, *104*, 4433–4440

23. Vácha, R.; Slavíček, P.; Mucha, M.; Finlayson-Pitts, B. J.; Jungwirth, P., *J. Phys. Chem. A* **2004**, *108*, 11573–11579
24. Martins-Costa, M. T. C.; Ruiz-López, M. F., *Chem. Phys*. **2007**, *332*, 341–347
25. Mortier, W. J.; Ghosh, S. K.; Shankar, S., *J. Am. Chem. Soc*. **1986**, *108*, 4315–4320
26. Rappe, A. K.; Goddard, W. A., *J. Phys. Chem*. **1991**, *95*, 3358–3363
27. Nalewajski, R. F., *Int. J. Quantum Chem*. **1992**, *42*, 243–265
28. Rick, S. W.; Stuart, S. J.; Berne, B. J., *J. Chem. Phys*. **1994**, *101*, 6141–6156
29. York, D. M.; Yang, W., *J. Chem. Phys*. **1996**, *104*, 159–172
30. Itskowitz, P.; Berkowitz, M. L., *J. Phys. Chem. A* **1997**, *101*, 5687–5691
31. Liu, Y. P.; Kim, K.; Berne, B. J.; Friesner, R. A.; Rick, S. W., *J. Chem. Phys*. **1998**, *108*, 4739–4755
32. Banks, J. L.; Kaminski, G. A.; Zhou, R.; Mainz, D. T.; Berne, B. J.; Friesner, R. A., *J. Chem. Phys*. **1999**, *110*, 741–754
33. Chelli, R.; Ciabatti, S.; Cardini, G.; Righini, R.; Procacci, P., *J. Chem. Phys*. **1999**, *111*, 4218–4229
34. Chelli, R.; Procacci, P.; Righini, R.; Califano, S., *J. Chem. Phys*. **1981**, *111*, 8569–8575
35. Chelli, R.; Procacci, P., *J. Chem. Phys*. **2002**, *117*, 9175–9199
36. Tabacchi, G.; Mundy, C. J.; Hutter, J.; Parrinello, M., *J. Chem. Phys*. **2002**, *117*, 1416–1433
37. Patel, S.; Brooks, C. L. 3rd, *J Comput Chem* **2004**, *25*, 1–15
38. Chelli, R.; Barducci, A.; Bellucci, L.; Schettino, V.; Procacci, P., *J. Chem. Phys*. **2005**, *123*, 194109
39. Chelli, R.; Pagliai, M.; Procacci, P.; Cardini, G.; Schettino, V., *J. Chem. Phys*. **2005**, *122*, 074504
40. Chelli, R.; Schettino, V.; Procacci, P., *J. Chem. Phys*. **2005**, *122*, 234107
41. Ishida, T.; Morita, A., *J. Chem. Phys*. **2006**, *125*, 074112
42. Piquemal, J. P.; Chelli, R.; Procacci, P.; Gresh, N., *J. Phys. Chem. A* **2007**, *111*, 8170–8176
43. Lee Warren, G.; Davis, J. E.; Patel, S., *J Chem Phys* **2008**, *128*, 144110.–144123
44. Zhong, Y.; Patel, S., *J. Phys. Chem. B* **2010**, *114*, 11076–11092
45. Yang, Z. Z.; Wang, C. S., *J. Phys. Chem. A* **1997**, *101*, 6315–6321
46. Wang, C. S.; Yang, Z. Z., *J. Chem. Phys*. **1999**, *110*, 6189–6197
47. Cong, Y.; Yang, Z. Z., *Chem. Phys. Lett*. **2000**, *316*, 324–329
48. Wu, Y.; Yang, Z. Z., *J. Phys. Chem. A* **2004**, *108*, 7563–7576
49. Yang, Z. Z.; Wu, Y.; Zhao, D. X., *J. Chem. Phys*. **2004**, *120*, 2541–2557
50. Li, X.; Yang, Z. Z., *J. Phys. Chem. A* **2005**, *109*, 4102–4111
51. Li, X.; Yang, Z. Z., *J. Chem. Phys*. **2005**, *122*, 084514
52. Yang, Z. Z.; Li, X., *J. Phys. Chem. A* **2005**, *109*, 3517–3520
53. Zhang, Q.; Yang, Z. Z., *Chem. Phys. Lett*. **2005**, *403*, 242–247
54. Yang, Z. Z.; Zhang, Q., *J. Comput. Chem*. **2006**, *27*, 1–10
55. Wang, F. F.; Gong, L. D.; Zhao, D. X., *J. Mol. Struct. THEOCHEM* **2009**, *909*, 49–56
56. Wang, F. F.; Zhao, D. X.; Gong, L. D., *Theor. Chem. Acc*. **2009**, *124*, 139–150
57. Wang, F. F.; Zhao, D. X.; Yang, Z. Z., *Chem. Phys*. **2009**, *360*, 141–149
58. Zhao, D. X.; Liu, C.; Wang, F. F.; Yu, C. Y.; Gong, L. D.; Liu, S. B.; Yang, Z. Z., *J. Chem. Theory Comput*. **2010**, *6*, 795–804
59. Yu, C. Y.; Yang, Z. Z., *J. Phys. Chem. A* **2011**, *115*, 2615–2626
60. Frisch, M. J.; Trucks, G. W.; Schlegel, H. B.; Scuseria, G. E.; Robb, M. A.; Cheeseman, J. R.; Montgomery, J. A. J.; Vreven, T.; Kudin, K. N.; Burant, J. C.; Millam, J. M.; Iyengar, S. S.; Tomasi, J.; Barone, V.; Mennucci, B.; Cossi, M.; Scalmani, G.; Rega, N.; Petersson, G. A.; Nakatsuji, H.; Hada, M.; Ehara, M.; Toyota, K.; Fukuda, R.; Hasegawa, J.; Ishida, M.; Nakajima, T.; Honda, Y.; Kitao, O.; Nakai, H.; Klene, M.; Li, X.; Knox, J. E.; Hratchian, H. P.; Cross, J. B.; Adamo, C.; Jaramillo, J.; Gomperts, R.; Stratmann, R. E.; Yazyev, O.; Austin, A. J.; Cammi, R.; Pomelli, C.; Ochterski, J. W.; Ayala, P. Y.; Morokuma, K.; Voth, G. A.; Salvador, P.; Dannenberg, J. J.; Zakrzewski, V. G.; Dapprich, S.; Daniels, A. D.; Strain, M. C.; Farkas, O.; Malick, D. K.; Rabuck, A. D.; Raghavachari, K.; Foresman, J. B.; Ortiz, J. V.; Cui, Q.; Baboul, A. G.; Clifford, S.; Cioslowski, J.; Stefanov, B. B.; Liu, G.; Liashenko, A.; Piskorz, P.; Komaromi, I.; Martin, R. L.; Fox, D. J.; Keith, T.; Al-Laham, M. A.; Peng, C. Y.; Nanayakkara, A.; Challacombe, M.; Gill, P. M. W.; Johnson, B.; Chen, W.; Wong, M. W.; Gonzalez, C.; Pople, J. A.; Revision D.01 ed.; Gaussian, Inc.: Wallingford, CT, 2004.
61. Boys, S. F.; Bernardi, F., *Mol. Phys*. **1970**, *19*, 553–566
62. Wang, C. S.; Li, S. M.; Yang, Z. Z., *J. Mol. Struct. THEOCHEM* **1998**, *430*, 191–199
63. Steinbach, P. J.; Brooks, B. R., *J. Comput. Chem*. **1994**, *15*, 667–683
64. Kurinovich, M. A.; Lee, J. K., *J. Am. Chem. Soc*. **2000**, *122*, 6258–6262